Inorganic Chemistry

Article

Cite This: Inorg. Chem. XXXX, XXX, XXX−XXX

pubs.acs.org/IC

Retention of a Paramagnetic Ground State at Low Temperatures in a Family of Structurally Related U^{IV} Phosphates

Justin B. Felder,[†] Stuart Calder,[‡] and Hans-Conrad zur Loye*[,†]

[†]Department of Chemistry and Biochemistry, University of South Carolina, Columbia, South Carolina 29208, United States

[‡]Neutron Scattering Division, Oak Ridge National Laboratory, Oak Ridge, Tennessee 27831, United States

Supporting Information

ABSTRACT: A new uranium fluoride phosphate, $UFPO_4$, was synthesized via a mild hydrothermal route and characterized optically, thermally, and magnetically. Two thermal transformation products, $U_2O(PO_4)_2$ and $U^{IV}U^{VI}O_2(PO_4)_2$, were discovered to be structurally related, and were subsequently synthesized for bulk property measurements. All three materials failed to follow Curie−Weiss behavior at low temperatures, attributed to the nearly ubiquitous singlet ground state of U(IV), transitioning into a Curie−Weiss paramagnetic regime at high temperatures. Neutron diffraction experiments were performed on $UFPO_4$ and $U^{IV}U^{VI}O_2(PO_4)_2$ in order to characterize this unusual magnetic behavior.

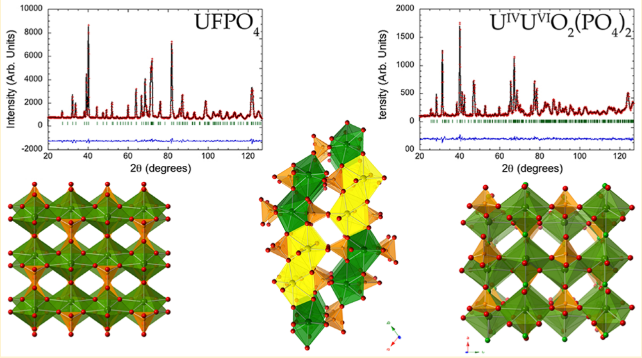

INTRODUCTION

Uranium chemistry has been investigated extensively since the 1940s when the focus was primarily on weapons and nuclear power applications. Only during the past few decades has there been time to broaden our understanding of uranium chemistry in general and to explore diverse classes of uranium containing materials, including oxides,[1] fluorides,[2] chalcogenides,[3] intermetallics,[4] and oxo-salt phases, such as phosphates.[5−8] The chemistry of uranium phosphates, in particular, has been extensively explored due to the existence of a multitude of known phosphate minerals. Synthesizing related phosphate materials in the laboratory has been achieved when using techniques that mimic nature's high-temperature, high-pressure solution environments. Specifically, the mild hydrothermal regime has yielded numerous new compositions, including fluorides[9] and phosphates. Although there is a relative dearth of U(IV) materials, uranium is well-known to form stable phosphate compounds. Phosphate groups have been shown to stabilize the tetravalent state of uranium, and the various polyoxo phosphorus ions interplay with U(IV) to create various structure types. In particular, there are known orthophosphates ($U_2O(PO_4)_2$, $U(UO_2)(PO_4)_2$),[10,11] pyrophosphates (UP_2O_7),[12] and triphosphates ($U_2(PO_4)(P_3O_{10})$).[13]

Uranium can exhibit a wide range of oxidation states (from +2 to +6), although only the +4 and +6 (and sometimes +5) oxidation states are readily accessible in solid-state materials.[14] The reduced +2 and +3 states are uncommon and unlikely to form under typical synthetic conditions. Although both the +4 and +6 oxidation states are found in nature, by far the majority of laboratory-synthesized uranium compounds found in the chemistry literature focus on U(VI) chemistry, which is dominated by the structure directing uranyl ($[O{=}U{=}O]^{2+}$) ion. While uranyl chemistry is a rich field that continues to produce interesting new materials,[15−17] exploring the synthesis of U(IV) containing materials is of particular interest as the U(IV) f^2 ion exhibits properties noticeably different from those found for the U(VI) f^0 ion. In addition, there are comparatively very few reported U(IV) containing materials, which makes this an attractive area to investigate.

Whereas the smaller U(VI) ion is fairly soluble, diamagnetic, and often fluorescent due to the uranyl ion, U(IV) is large, insoluble, paramagnetic, and has optical properties dominated by f−f electronic transitions. Among these properties, the magnetism of U(IV) is by far the most intriguing. U(IV) is a $5f^2$ system whose magnetism arises from a combination of spin−orbit interactions and crystal field effects.[18,19] These spin−orbit effects are primarily due to low-lying thermally excited f states that can become depopulated at low temperatures. This thermal depopulation leads to formation of a diamagnetic singlet ground state, which is extremely prevalent among reported U(IV) materials.[2,20−22]

Since the magnetism of U(IV) materials is also dependent on crystal field effects, it should be possible to influence the transition to the singlet state by controlling the structure and composition, which in turn will determine the crystal electric field. Chemists are extremely good at controlling composition, less so, however, at controlling structure and crystal-field effects. Nonetheless, it is not surprising that when exploring the U(IV) phase space one should encounter materials that have rather unique crystal-field effects as evidenced by their magnetic behavior. Herein we report the preparation and magnetic studies

Received: May 10, 2018

DOI: 10.1021/acs.inorgchem.8b01284
Inorg. Chem. XXXX, XXX, XXX−XXX

of three related uranium(IV) phosphates, $UFPO_4$, $U_2O(PO_4)_2$, and $U^{IV}U^{VI}O_2(PO_4)_2$, that are structurally closely related, share almost identical coordination environments, exhibit unusual magnetic behavior, and therefore provide us with an opportunity to further investigate the influence of coordination environment on U(IV) magnetism.

■ EXPERIMENTAL SECTION

Materials and Methods. The following materials were used as received with no further modification: $UO_2(CH_3COO)_2$, FeF_3, H_3PO_4, $NH_4H_2PO_4$, and U_3O_8. UO_2 was synthesized by reducing the U_3O_8 under a 4% H_2 atmosphere at 650 °C for 18 h. UO_2 was confirmed pure by PXRD.

Caution! *Even though the uranium precursors used in these syntheses are depleted, standard precautions and PPE for handling radioactive materials should be followed. All work involving uranium was performed in laboratories specially designated for work with radioactive materials.*

$UFPO_4$ was synthesized via a mild hydrothermal reaction between uranyl acetate and phosphoric acid, with iron(III) fluoride acting as a fluoride source. The uranyl acetate and iron(III) fluoride were mixed with 1 mL of methanol in a 23 mL PTFE liner. Next, 1 mL of concentrated phosphoric acid was added dropwise to the mixture, and the liner was sealed inside a stainless-steel autoclave. The sealed autoclave was placed into a programmable oven that was heated to 200 °C in 1 h, then held for 24 h followed by slow cooling at a rate of 0.1°/min to 40 °C, at which point the oven was shut off. After cooling to room temperature, the autoclave was unsealed and the liner opened, revealing emerald-green product crystals and a green mother liquor. The crystals were isolated by vacuum filtration and washed thoroughly with water and acetone. After isolation, the crystals were all found to be of similar size, ~0.1 mm on edge.

$U^{IV}U^{VI}O_2(PO_4)_2$ was synthesized by a flux-assisted solid-state reaction between P_2O_5 and UO_2. The P_2O_5 was generated *in situ* by decomposing ammonium dihydrogen phosphate at 450 °C. Stoichiometric amounts of UO_2 and $NH_4H_2PO_4$ were ground together in an agate mortar, producing an intimate mixture of powders. The powders were loaded into a fused silica tube, which was placed in a box furnace. The furnace was heated to 450 °C in 12 h and held at that temperature for an additional 24 h. Subsequently, the furnace was slowly heated to 800 °C over a period of 12 h to ensure the slow removal of ammonia gas. The charge was held at 800 °C for 24 h after which point the furnace was shut off. The product was removed from the tube, ground, and heated at 850 °C for 24 h. This was repeated twice to yield pure $U^{IV}U^{VI}O_2(PO_4)_2$. Samples of $U_2O(PO_4)_2$ were synthesized by reducing $U^{IV}U^{VI}O_2(PO_4)_2$ in a 4% H_2/96% N_2 mixture at 650 °C for 18 h.

Single Crystal X-ray Diffraction. A suitable crystal of the green product was selected from the reaction products and X-ray intensity data were collected using a Bruker D8 QUEST diffractometer. The instrument utilizes an incoatec microfocus X-ray source (Mo Kα radiation, $\lambda = 0.71073$ Å) and a PHOTON II CMOS area detector. The detector was operated in the shutterless mode, and additional fast scans were collected to account for overtopped pixels during the initial data collection. The final unit cell parameters were determined by least-squares refinement of a large set of reflections taken from the raw area detector frames. The data were reduced and corrected for absorption effects using the SAINT+ and SADABS programs.[23] An initial structural model was obtained using SHELXS[24] by direct methods, and subsequent least-squares refinements were performed with SHELXL[24] through the OLEX^2[25] graphical interface.

The observed lattice parameters were found to be very similar to $NpFPO_4$, which was previously reported by Albrecht-Schmitt.[26] The measured crystal was determined to be isostructural with $NpFPO_4$, crystallizing in the orthorhombic space group *Pnma*. The data refined well to an R_1 value of 1.76%. The largest peak and hole are 2.30 and −1.98 $e^-/Å^3$ respectively. Selected crystallographic and refinement information for $UFPO_4$ can be found in Table 1.

Table 1. Crystallographic and Refinement Data for $UFPO_4$

empirical formula	F O_4 P U
formula weight	352.00 g/mol
temperature	310.52 K
crystal system	orthorhombic
space group	*Pnma*
a	8.6377(2)
b	6.9826(2)
c	6.3607(2)
volume	383.637(19) $Å^3$
Z	4
density	6.095 g/cm^3
absorption coefficient	42.636 mm^{-1}
F(000)	592.0
crystal size	0.078 mm × 0.076 mm × 0.022 mm
wavelength	0.71073 Å
2θ range for data collection	7.958−72.624°
reflections collected	32820
independent reflections	987
data/restraints/parameters	987/0/41
goodness of fit on F^2	1.492
final *R* indices (all data)	$R_1 = 0.0176$; $wR_2 = 0.0428$
largest diff. peak and hole	2.30/−1.98 $e^-/Å^3$

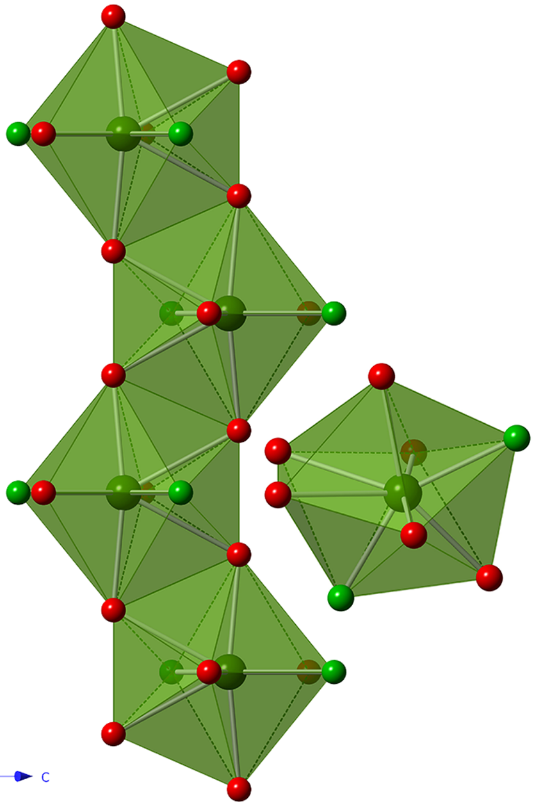

Figure 1. Fragment of the infinite uranium oxyfluoride chains that make up the structure of $UFPO_4$ (left). Each UO_6F_2 polyhedron (right) shares two edges of oxygen ligands to form the infinite chains running along the *b* direction. Uranium is shown as green polyhedra, oxygen is shown as red spheres, and fluorine is shown as green spheres.

Powder X-ray Diffraction. PXRD patterns were collected on a Rigaku Ultima IV diffractometer using Cu Kα radiation ($\lambda = 1.5418$ Å) and a D/Tex high speed detector. Patterns were collected in the angular range of 5−65° 2θ with a step size of 0.02°.

Neutron Powder Diffraction. Neutron powder diffraction (NPD) patterns of $UFPO_4$ and $U^{IV}U^{VI}O_2(PO_4)_2$ were collected on beamline HB-2A (POWDER) at ORNL's HFIR site. Patterns were collected

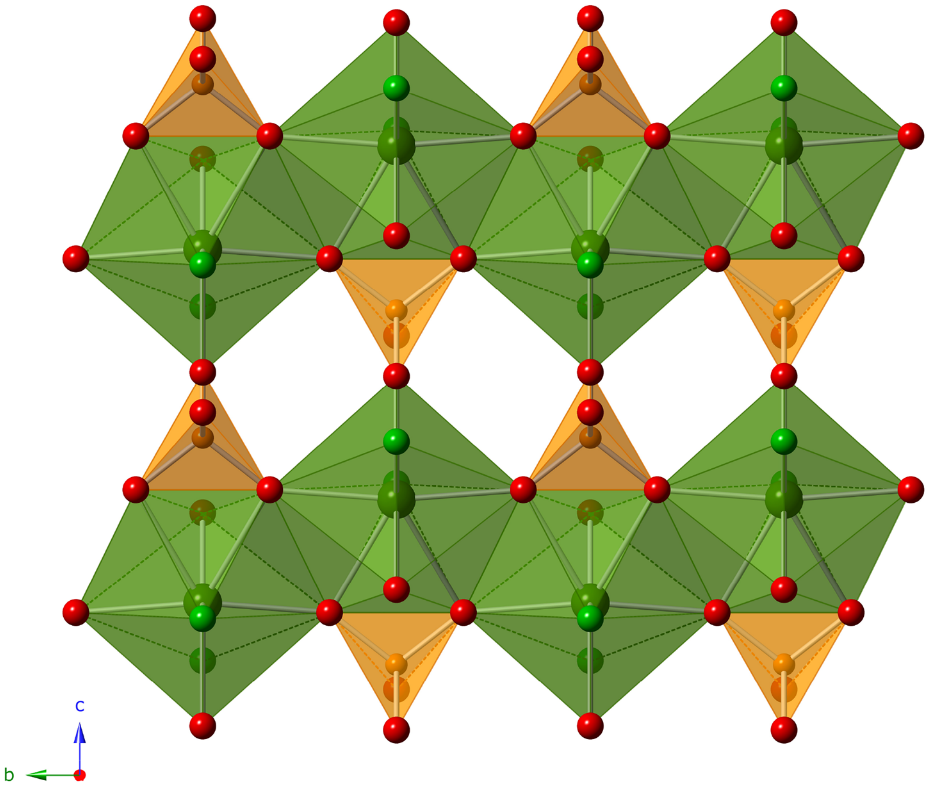

Figure 2. Edge-sharing uranium chains decorated by phosphate tetrahedra. The chains are connected along the *c* direction forming "sheets" of linked chains. The (apparently) unbonded phosphate oxygens shown here serves to bridge these sheets along the *a* direction (not shown). Uranium is shown as green polyhedra, phosphorus is shown as orange tetrahedra, oxygen is shown as red spheres, and fluorine is shown as green spheres.

using a bank of 44 ^{3}He detectors. Data were collected in the 20−130° 2θ range with a step size of 0.05°. Magnetic contributions were probed using neutrons with a wavelength of 2.41 Å to obtain good resolution at low *Q*.

Thermogravimetric Analysis. Thermal properties were probed using TGA under flowing N_2 or H_2 (4% in 96%N_2; 100 mL/min) from room temperature to 800 or 900 °C. The thermal products were characterized by PXRD and were used to guide the syntheses of $U_2O(PO_4)_2$ and $U^{IV}U^{VI}O_2(PO_4)_2$.

SQUID Magnetometry. Magnetic susceptibility data were collected using a Quantum Design MPMS3 SQUID magnetometer using polycrystalline powders obtained by grinding as-synthesized single crystals. Magnetic susceptibilities were measured in an applied field of 0.1 T in the 2−400 K temperature range. The data were corrected for shape and radial offset effects using previously described methods.[27]

■ RESULTS AND DISCUSSION

Powder X-ray Diffraction. Each of the synthesized compounds was characterized by PXRD to confirm the phase purity of the target composition. The PXRD patterns of $UFPO_4$, $U_2O(PO_4)_2$, and $U^{IV}U^{VI}O_2(PO_4)_2$ are shown in Figure S1.

Synthesis of $UFPO_4$. Although the mild hydrothermal method has proven extremely effective for synthesizing new uranium fluorides, the abundance of aqua ligands available in these systems frequently results in hydrated materials, which limit thermal stability and due to the presence of hydrogen make characterization techniques such as neutron diffraction quite difficult. In order to avoid this, a solvothermal approach using a methanol/phosphoric acid solution was employed to limit the amount of water available to the system. In addition, the solubility of many metal species is lower in methanol than in water; therefore, we expect to observe different crystalline products upon switching solvent systems.

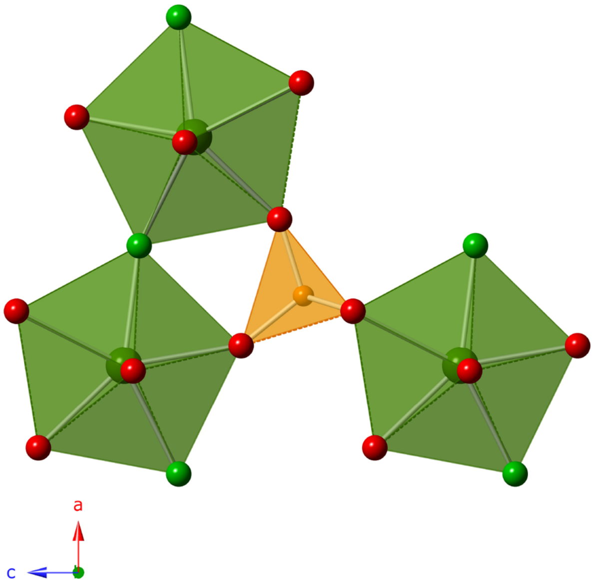

Figure 3. Tetranuclear cluster of uranium polyhedra bridged by a phosphate tetrahedron. This illustrates how the uranium oxyfluoride chains (running along the *b* direction) are connected in the *a* direction by fluoride bridges, and both in the *a* and *c* directions by phosphate bridges. Uranium is shown as green polyhedra, phosphate is shown as orange polyhedra, oxygen is shown as red spheres, and fluorine is shown as green spheres.

The use of concentrated HF (48%), while an excellent fluorine source, would introduce a large quantity of water to the system, and therefore an alternate source of fluorine was desired. We explored using alkali and alkaline earth metal fluorides as

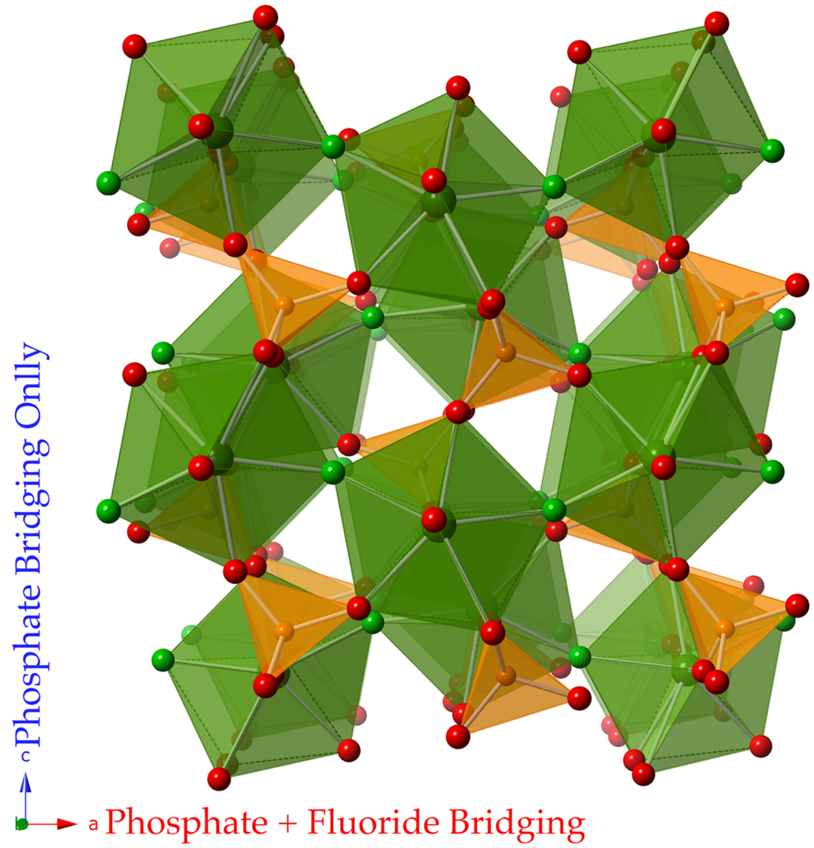

Figure 4. Overall structure of $UFPO_4$ as viewed down the *b* axis. The uranium chains running along the *b* direction are bridged in the *c* direction only by phosphate groups, while they are bridged in the *a* direction by both phosphate groups and fluoride ligands. Uranium is shown as green polyhedra, phosphorus is shown as orange polyhedra, oxygen is shown as red spheres, and fluorine is shown as green spheres.

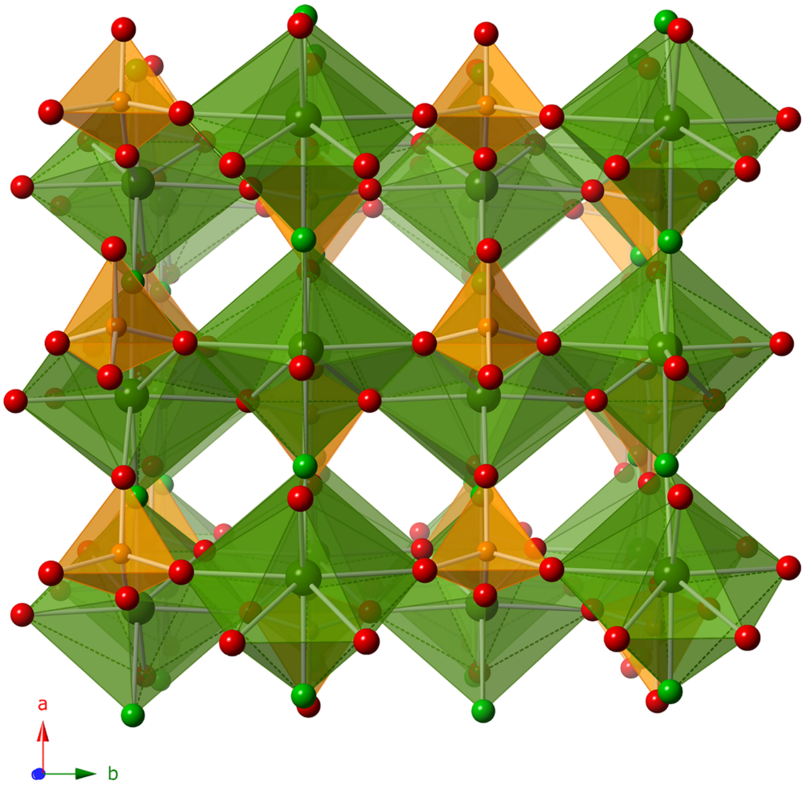

Figure 5. View of $UFPO_4$ down the *c* axis. This view of the structure accentuates the presence of the infinite uranium oxyfluoride chains running parallel to the *b* direction. Uranium polyhedra are shown in green, phosphorus is shown in orange, oxygen is shown as red spheres, and fluorine is shown as green spheres.

DOI: 10.1021/acs.inorgchem.8b01284
Inorg. Chem. XXXX, XXX, XXX−XXX

soluble fluorine sources; however, the introduction of these materials resulted consistently in $U_3F_{12}\cdot H_2O$, a previously reported phase.[28] We hypothesize that the reduction of U(VI) to U(IV) via the organic reducing agent, acetate, happens quickly and that the thus created U(IV) quickly reacts with the available F^- ions and crashes out as the stable $U_3F_{12}\cdot H_2O$ phase. By introducing the less soluble (slow-release) FeF_3 as a fluorine source, we ensure that the U(IV) has time to interact with other anions in solution (i.e., phosphate) before being fluorinated and crystallizing. This method proved successful, and the anhydrous $UFPO_4$ resulted from these synthetic trials.

Crystal Structure of $UFPO_4$. $UFPO_4$ is a three-dimensional structure built of cross-linked uranium oxyfluoride chains. Phosphate groups serve as an additional linkage between the chains. The chains are built primarily of $UO_{6/2}F_{2/2}$ 8-coordinate polyhedra. The local environment of a single UO_6F_2 polyhedron as well as of one chain fragment are shown in Figure 1. Each uranium ion is coordinated by 6 oxygen and 2 fluorine ions. Four of the oxygens lie in an equatorial plane and connect the polyhedra into chains via edge sharing. The remaining two oxygen and two fluorine ligands lie in a perpendicular plane with the fluorine ions arranged roughly *trans* to one another. Each chain is decorated with phosphate tetrahedra such that all phosphate oxygen atoms are shared between uranium and phosphorus. Figure 2 depicts the phosphate decorated uranium chain and shows how two chains are bridged by phosphate tetrahedra in the *c* direction.

The tetrahedral nature of the phosphate groups causes the chains shown in Figure 2 to be connected into corrugated sheets. These corrugated sheets in turn are connected in the *a* direction by a combination of phosphate and fluoride bridging groups/ligands. Figure 3 shows the connectivity in the *a* direction. Figure 4 shows the complete structure viewed down the *b* direction to emphasize the connectivity of uranium chains. Figure 5 depicts a different orientation to provide a complete view of the structure down the *c* axis.

Thermal Behavior of $UFPO_4$. The thermal properties of $UFPO_4$ were initially investigated by heating $UFPO_4$ to 800 °C under nitrogen flow. The TG curve reveals a smooth weight loss beginning immediately upon heating and leveling off at 800 °C. A plot of the TGA data is shown in Figure 6. The material obtained by heating $UFPO_4$ to 800 °C and cooling back down to room temperature was analyzed by PXRD and found to consist of a mixture of $U_2O(PO_4)_2$ and several unidentified phases. The primary phase, $U_2O(PO_4)_2$, was found to be structurally closely related to $UFPO_4$, and attempts were made to prepare and isolate a pure sample of $U_2O(PO_4)_2$. This was initially attempted by heating $UFPO_4$ to 900 °C in the anticipation that the higher temperatures would drive the transformation to completion; this, however, instead resulted in another structurally related phosphate, $U^{IV}U^{VI}O_2(PO_4)_2$. A plot of the TGA data is shown in Figure 6. The second attempt involved heating $UFPO_4$ under a 4% hydrogen atmosphere at 800 °C. These TGA results are shown in Figure 6 and reveal that the primary product was the desired $U_2O(PO_4)_2$; however, some small impurity phases persist. Figure S2 shows the post-TGA XRD patterns for the three discussed TGA runs. To obtain pure samples of both $U_2O(PO_4)_2$ and $U^{IV}U^{VI}O_2(PO_4)_2$ in order to fully investigate their physical properties and to compare them to $UFPO_4$, they were prepared via solid-state reactions.

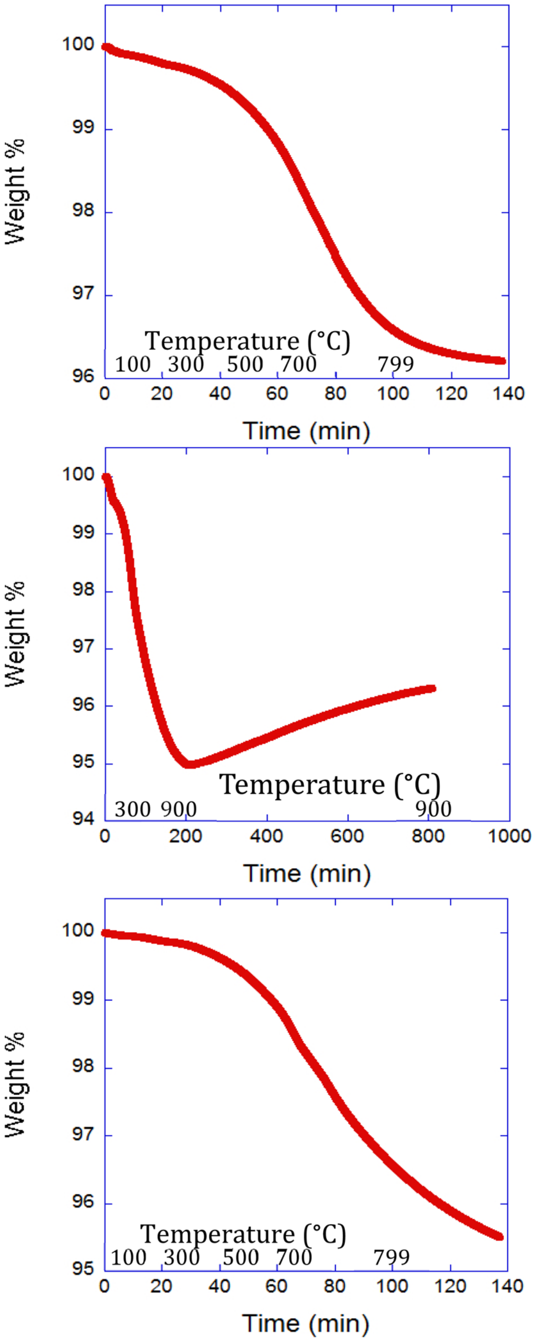

Figure 6. Top: TG curve of $UFPO_4$ from room temperature to 800 °C under a N_2 gas flow. $UFPO_4$ loses weight continuously until 800 °C at which point it levels out. Middle: TG curve of $UFPO_4$ from room temperature to 900 °C under flowing N_2, followed by a 12 h isothermal hold at 900 °C. $UFPO_4$ loses weight until 900 °C, at which point it begins to gain weight, presumably due to the oxidation of one U atom from IV to VI and the concomitant uptake of oxygen. Bottom: TG curve of $UFPO_4$ from room temperature to 800 °C under a 4% H_2 atmosphere. $UFPO_4$ loses weight to 800 °C at which point it begins to stabilize.

Synthesis of $U^{IV}U^{VI}O_2(PO_4)_2$. In order to synthesize the uranium uranyl phosphate material, we made use of a previously reported flux-assisted solid-state synthesis.[29] In this method, stoichiometric amounts of UO_2 and $NH_4H_2PO_4$ are combined in a fused silica tube. The charge is heated according to the profile given in the Experimental Section. This profile initially leads to the formation of P_2O_5 at 450 °C as the ammonia and water vapor are driven off the phosphate. Once this process is complete, the charge is heated to 800 °C, which renders the

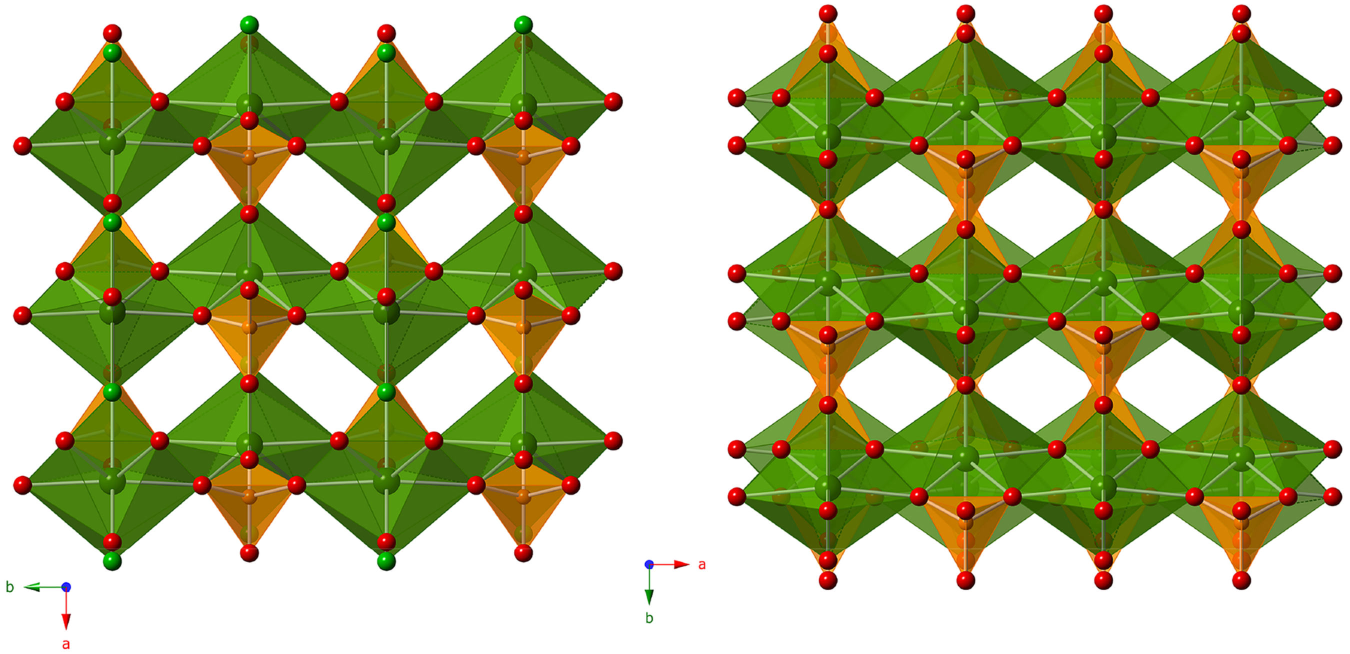

Figure 7. Side by side comparison of $UFPO_4$ (left) with $U_2O(PO_4)_2$ (right). The primary structural consequences of the transformation are the lowering of the coordination number of uranium from 8 to 7 and a slight rearrangement of the uranium chains. This rearrangement is primarily due to the decreased coordination number which removes half of the interchain U−U bridges (through F in $UFPO_4$, O in $U_2O(PO_4)_2$). Uranium is shown in green, phosphate is shown in orange, oxygen is shown in red, and fluorine is shown in light green.

P_2O_5 molten allowing it to react efficiently with the uranium. This initial reaction yields a mixture of unidentified phases. To homogenize the material and to obtain phase pure $U^{IV}U^{VI}O_2(PO_4)_2$, the sample is ground and heated twice more at 850 °C with one intermediate grinding, resulting in phase pure $U^{IV}U^{VI}O_2(PO_4)_2$. The PXRD pattern confirming phase purity is shown in Figure S1.

Synthesis of $U_2O(PO_4)_2$. Since these three uranium phosphates are structurally related, we reasoned that interconversion between these phases should be possible. $U_2O(PO_4)_2$ contains only one fewer oxide ion than $U^{IV}U^{VI}O_2(PO_4)_2$, suggesting it should be possible to reduce $U^{IV}U^{VI}O_2(PO_4)_2$ to form the $U_2O(PO_4)_2$ phase. To test this, freshly made $U^{IV}U^{VI}O_2(PO_4)_2$ was heated under a 4% H_2 flow at 650 °C for 18 h. This resulted in a pure sample of $U_2O(PO_4)_2$ as evidenced by the PXRD pattern shown in Figure S1.

Structural Comparison of $U_2O(PO_4)_2$ and $U^{IV}U^{VI}O_2(PO_4)_2$ with $UFPO_4$. Although the structures of $U_2O(PO_4)_2$ and $U^{IV}U^{VI}O_2(PO_4)_2$ have been reported elsewhere[29,30] (ICSD numbers 402120 and 75358 respectively), they will be discussed briefly for the purpose of comparing them to the structure of $UFPO_4$. The structure of $U_2O(PO_4)_2$ is nearly identical to that of $UFPO_4$. Conceptually, doubling the unit cell of $UFPO_4$ in the c direction results in $U_2F_2(PO_4)_2$). Replacing the two fluoride ions with one oxide ion, to maintain charge balance, results in $U_2O(PO_4)_2$. This transformation effectively reduces the coordination number of uranium from 8 to 7 and results in a slight rearrangement of the uranium chains from an eclipsed to a staggered arrangement. Figure 7 shows the comparison between $UFPO_4$ and $U_2O(PO_4)_2$.

$U^{IV}U^{VI}O_2(PO_4)_2$ is structurally also closely related to $UFPO_4$ and $U_2O(PO_4)_2$, and the existing differences arise primarily from the fact that half of the U atoms are U(VI) rather than all U(IV), as is the case in both $UFPO_4$ and $U_2O(PO_4)_2$. The simultaneous presence of U(IV) and U(VI) results in charge-ordering, where the uranium atoms are arranged in dimers: alternating $U^{4+}-U^{4+}-U^{6+}-U^{6+}-U^{4+}-U^{4+}$ and so on. All of the U atoms remain in a 7-coordinate environment; however, the polyhedra change from somewhat irregular UO_7 polyhedra in $U_2O(PO_4)_2$ to fairly regular pentagonal bipyramids (as would be expected for the uranyl ions) in $U^{IV}U^{VI}O_2(PO_4)_2$. The assignment of U(IV) versus U(VI) can easily be made by comparing the lengths of the uranyl bonds (1.7 Å) to the axial bonds of U(IV) (2.1 Å) in this structure. The oxidation of one of the uranium atoms results in the loss of U−O−U interchain bonding, which is a consequence of the now inert uranyl oxygens that cannot form the connection. The phosphate tetrahedra are still present in a more or less unchanged location and still serve to connect the uranium chains. All three reported structures are shown for comparison in Figure 8.

Structural Comparison of $UFPO_4$ with $UXPO_4{\cdot}2H_2O$ (X = Cl, Br). It should be noted that in addition to the anhydrous $UFPO_4$ reported here there exist two additional U(IV) halide phosphates ($UClPO_4$, and $UBrPO_4$) both dihydrates.[31] These materials exist as sheet-type structures with the U(IV)−phosphate bridges forming two-dimensional rings. These rings are bridged together by P−O bonds forming a 3D network. These two tetragonal structures are distinct from the $UFPO_4$ structure described above. The difference in structure might be attributed to the greater propensity of Cl and Br to form terminal bonds compared to F.

Interestingly, the local coordination environments of uranium in these halide phosphates are more closely related to those of uranium in $U_2O(PO_4)_2$ and $U(UO_2)(PO_4)_2$, which were described earlier. All four of these local uranium environments are based on the pentagonal bipyramidal geometry; however, the halogen ion in the $UXPO_4$ phases causes the geometry to be quite distorted.

Magnetic Susceptibility of $UFPO_4$, $U_2O(PO_4)_2$, and $U^{IV}U^{VI}O_2(PO_4)_2$. Since U(IV) is a $5f^2$ magnetic ion, we expect

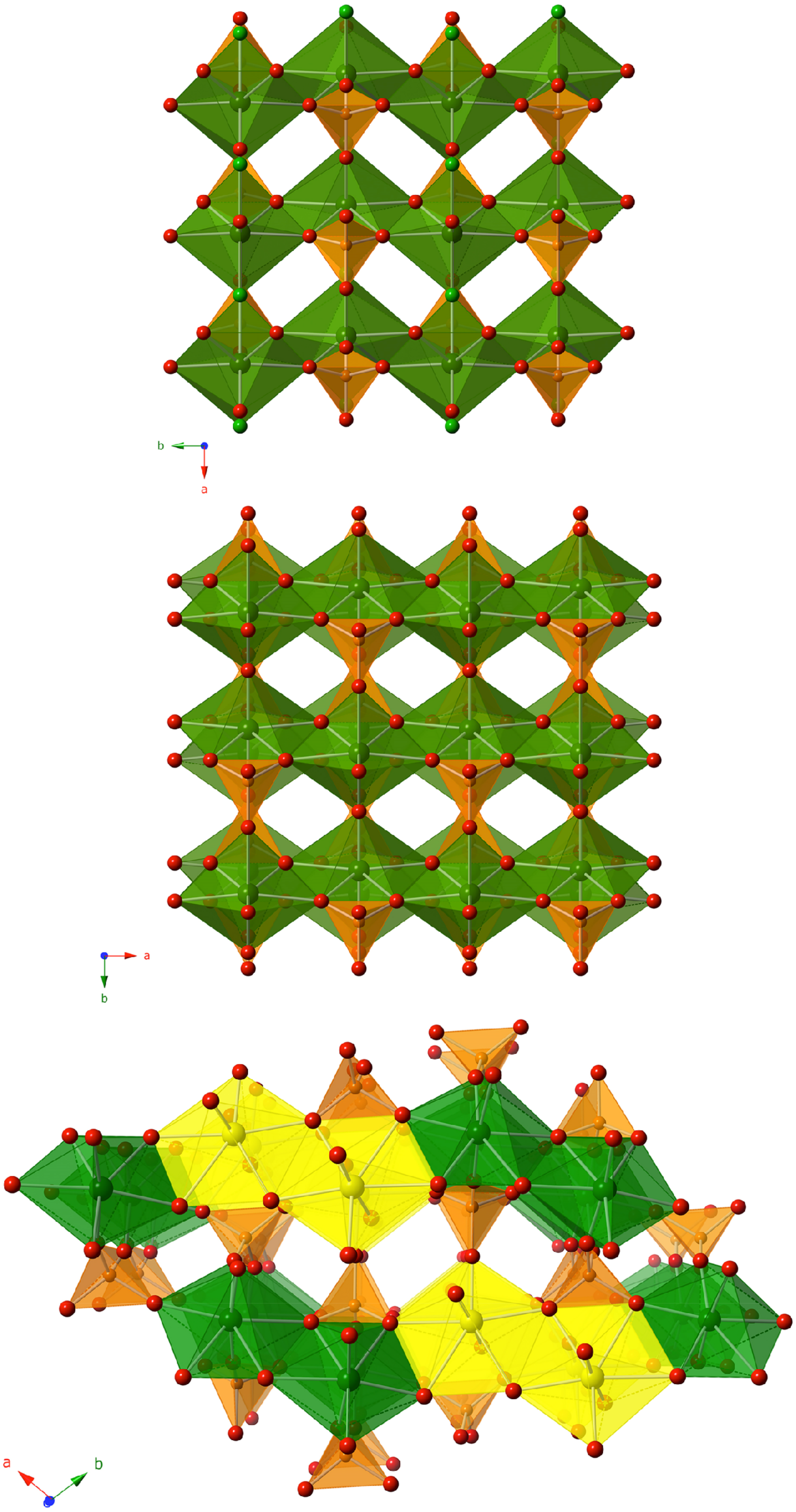

Figure 8. Comparison of the structures of $UFPO_4$ (top), $U_2O(PO_4)_2$ (middle), and $U(UO_2)(PO_4)_2$ (bottom). In $U(UO_2)(PO_4)_2$ there are two uranyl ions that alternate with two U(IV) ions. U(IV) is shown in green, U(VI) is shown in yellow, phosphorus is shown in orange, oxygen is shown in red, and fluorine is shown in light green.

both crystal-field and spin−orbit effects to contribute to the size of the magnetic moment. Furthermore, the close similarity of the three reported structures provides us with a unique opportunity to probe how small changes in coordination environment affect the magnetism of U(IV). In $UFPO_4$, there are multiple possible magnetic exchange pathways: U−O−U interactions through edge shared members of the uranium chains, U−F−U interactions between chains and U−O−P−O−U super-superexchange interactions between chains. In $U_2O(PO_4)_2$, these interactions are slightly simplified as half of the U−F−U interactions (now additional U−O−U) have been removed by the doubling of the *c* axis. Finally, $U^{IV}U^{VI}O_2(PO_4)_2$ removes the U−O−U interchain interaction altogether, as well as removes long-range U−O−U intrachain interactions, as the chains are now interrupted by diamagnetic uranyl ions. The primary magnetic interactions in this material are therefore U−O−U dimer interactions. These dimers can interact via super-superexchange through phosphate groups along the *a* axis.

The magnetic susceptibility of all three materials are shown in Figure 9. All three materials exhibit an increase in their susceptibility, to varying degree, at low temperatures. $UFPO_4$ exhibits the most dramatic increase and is reminiscent of a paramagnet, while the upturns in $U_2O(PO_4)_2$ and $U^{IV}U^{VI}O_2(PO_4)_2$ are more subtle. This behavior is not consistent with the singlet ground state that is common among U(IV) materials, although the exact nature of the magnetism cannot be determined using the SQUID data alone. For that reason, powder neutron diffraction was performed to probe the potential presence of magnetic order.

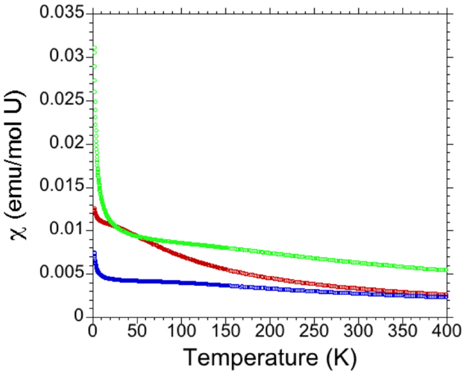

Figure 9. Magnetic susceptibilities of $UFPO_4$ (green), $U_2O(PO_4)_2$ (red), and $U(UO_2)(PO_4)_2$ (blue). The susceptibilities have been normalized to represent the magnetic susceptibility per U(IV) ion to make the values directly comparable.

U(IV) typically does not obey the Curie−Weiss law at low temperatures, which makes obtaining an effective moment somewhat difficult. In order to determine effective high temperature moments, a plot of $2.827(\chi_m \cdot T)^{1/2}$ versus T was generated (Figure 10). This plot yields effective moments of 4.2 μ_B/U for $UFPO_4$, 2.9 μ_B/U for $U_2O(PO_4)_2$, and 2.7 μ_B/U(IV) for $U^{IV}U^{VI}O_2(PO_4)_2$ at 300 K. U(IV) typically displays moments of 3.5−3.9 μ_B,[12] meaning these values are slightly outside the reported range (although this is not uncommon). Nonetheless, these results exemplify how significant structural changes around the U(IV) ion effect small changes in the crystal fields and hence the magnetic moment of 5f magnetic systems.

NPD of $UFPO_4$ and $U^{IV}U^{VI}O_2(PO_4)_2$. $UFPO_4$ exhibits a moment higher than expected based on the reported range of moments, and for that reason, the potential for the existence of magnetic correlations was considered. As no obvious magnetic transition was observed in the magnetic susceptibility data, NPD data of $UFPO_4$ and $U^{IV}U^{VI}O_2(PO_4)_2$ were collected at different temperatures and analyzed for the presence of any magnetic contribution. NPD patterns collected at 4 and 300 K were overlaid and found to be identical except for the expected thermal lattice expansion. No additional peaks or changes in peak intensity that would indicate the presence of magnetic ordering were observed. The NPD patterns were fit to structural models using the Rietveld method, and the structural models were found to account very well for all of the observed NPD peak intensity. Figure 11 depicts the Rietveld plots for $UFPO_4$ and $U^{IV}U^{VI}O_2(PO_4)_2$. No significant changes to the initial structural models were observed. Selected refinement parameters are listed in Table 2. On the basis of these data, we conclude that no magnetic order is present in $UFPO_4$ and $U^{IV}U^{VI}O_2(PO_4)_2$.

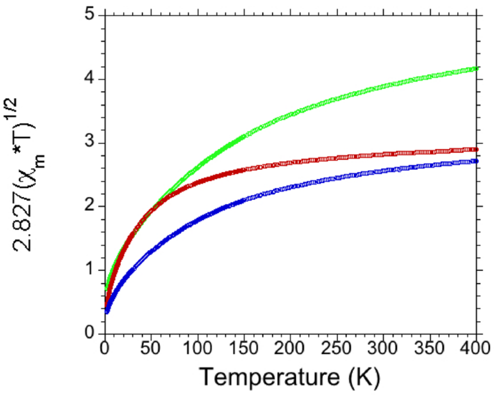

Figure 10. $\chi_m \cdot T$ vs T plots for $UFPO_4$ (green), $U_2O(PO_4)_2$ (red), and $U(UO_2)(PO_4)_2$ (blue). The moments decrease with decreasing temperature, consistent with a loss of thermally excited f states; however, the moments never reach 0, which would be indicative of a singlet ground state.

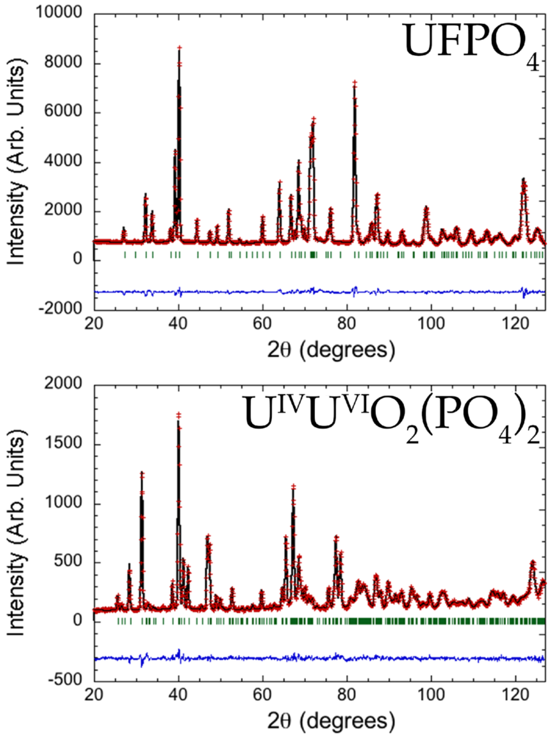

Figure 11. Rietveld refinements of the neutron diffraction data of $UFPO_4$ and $U(UO_2)(PO_4)_2$ collected at 4 K. Neutrons with $\lambda = 2.41$ Å were used to probe the presence of any magnetic order.

■ CONCLUSIONS

Magnetic susceptibility data indicate that $UFPO_4$ with its high coordination number and large number of magnetic exchange

Table 2. Selected Rietveld Statistics for $UFPO_4$ and $U(UO_2)(PO_4)_2$

	$UFPO_4$	$U(UO_2)(PO_4)_2$
a	8.67587(9)	8.8265(2)
b	7.00931(6)	9.2339(2)
c	6.37931(7)	5.4760(1)
α	90	102.662(2)
β	90	97.705(2)
γ	90	102.366(2)
χ^2	11.9%	3.16%
R_p	2.33	3.91
R_{wp}	3.13	5.13

pathways exhibits a clear retention of a paramagnetic state down to 2 K. In addition, $UFPO_4$ exhibits a magnetic moment that is higher than expected based on previously reported moments for U(IV). Neutron diffraction experiments, however, did not reveal the presence of any magnetic ordering.

A comparison of the magnetic behavior of $UFPO_4$ with those of $U_2O(PO_4)_2$ and $U^{IV}U^{VI}O_2(PO_4)_2$ is made difficult by the presence of multiple structural differences; however, both $U_2O(PO_4)_2$ and $U^{IV}U^{VI}O_2(PO_4)_2$ clearly exhibit magnetic moments almost a full Bohr magneton lower than the expected values and significantly lower than that of $UFPO_4$, whose moment is higher than expected. While more data are needed to establish a pattern of uranium(IV) coordination environments and magnetic moments, it is nonetheless obvious from this study that the coordination environment of uranium plays a direct role in the magnetic behavior of U(IV) containing materials.

■ ASSOCIATED CONTENT

Ⓢ Supporting Information

The Supporting Information is available free of charge on the ACS Publications website at DOI: 10.1021/acs.inorgchem.8b01284.

> $UFPO_4$, PXRD patterns for all reported materials, and post-TGA PXRD patterns for the thermal products of all three reported materials (PDF)

Accession Codes

CCDC 1842529 contains the supplementary crystallographic data for this paper. These data can be obtained free of charge via www.ccdc.cam.ac.uk/data_request/cif, or by emailing data_request@ccdc.cam.ac.uk, or by contacting The Cambridge Crystallographic Data Centre, 12 Union Road, Cambridge CB2 1EZ, UK; fax: +44 1223 336033.

■ AUTHOR INFORMATION

Corresponding Author

*E-mail: zurloye@mailbox.sc.edu.

ORCID

Hans-Conrad zur Loye: 0000-0001-7351-9098

Notes

The authors declare no competing financial interest.

■ ACKNOWLEDGMENTS

We gratefully acknowledge the United States Department of Energy, Office of Basic Energy Sciences, Division of Materials Sciences and Engineering for funding this work through award DE-SC0008664 and DE-SC0018739. The work at ORNL was funding by the United States Department of Energy, Office of Basic Energy Sciences.

■ REFERENCES

(1) Pace, K. A.; Kocevski, V.; Karakalos, S. G.; Morrison, G.; Besmann, T.; zur Loye, H.-C. $Na_2(UO_2)(BO_3)$: An All-Uranium(V) Borate Synthesized under Mild Hydrothermal Conditions. *Inorg. Chem.* **2018**, *57*, 4244−4247.

(2) Yeon, J.; Smith, M. D.; Tapp, J.; Möller, A.; zur Loye, H.-C. Application of a Mild Hydrothermal Approach Containing an in Situ Reduction Step to the Growth of Single Crystals of the Quaternary U(IV)-Containing Fluorides $Na_4MU_6F_{30}$ ($M = Mn^{2+}$, Co^{2+}, and Zn^{2+}) Crystal Growth, Structures, and Magnetic Properties. *J. Am. Chem. Soc.* **2014**, *136*, 3955−3963.

(3) Prakash, J.; Tarasenko, M. S.; Mesbah, A.; Lebègue, S.; Malliakas, C. D.; Ibers, J. A. Synthesis, Crystal Structure, Theoretical, and Resistivity Study of $BaUSe_3$. *Inorg. Chem.* **2016**, *55*, 7734−7738.

(4) Prokeš, K.; de Visser, A.; Huang, Y. K.; Fåk, B.; Ressouche, E. Anomalous spin distribution in the superconducting ferromagnet UCoGe studied by polarized neutron diffraction. *Phys. Rev. B: Condens. Matter Mater. Phys.* **2010**, *81*, 1473.

(5) Juillerat, C. A.; Moore, E. E.; Besmann, T.; zur Loye, H.-C. Observation of an Unusual Uranyl Cation-Cation Interaction in the Strongly Fluorescent Layered Uranyl Phosphates $Rb_6[(UO_2)_7O_4(PO_4)_4]$ and $Cs_6[(UO_2)_7O_4(PO_4)_4]$. *Inorg. Chem.* **2018**, *57*, 3675−3678.

(6) Brandel, V.; Dacheux, N.; Genet, M. Reexamination of U(IV) Phosphate Chemistry. *J. Solid State Chem.* **1996**, *121*, 467−472.

(7) Brandel, V.; Dacheux, N. Chemistry of Tetravalent Actinide Phosphates - Part I. *J. Solid State Chem.* **2004**, *177*, 4743−4754.

(8) Brandel, V.; Dacheux, N. Chemistry of Tetravalent Actinide Phosphates - Part II. *J. Solid State Chem.* **2004**, *177*, 4755−4767.

(9) Klepov, V. V.; Felder, J. B.; zur Loye, H.-C. Synthetic Strategies for the Synthesis of Ternary Uranium(IV) and Thorium(IV) Fluorides. *Inorg. Chem.* **2018**, *57*, 5597−5606.

(10) Benard, P.; Louer, D.; Dacheux, N.; Brandel, V.; Genet, M. Synthesis, ab initio structure determination from powder diffraction and spectroscopic properties of a new diuranium oxide phosphate. *An. Quim.* **1996**, *92*, 79−87.

(11) Albering, J. H.; Jeitschko, W. Crystal structure of diuranium monoxide diorthophosphate, $(U_2O)(PO_4)_2$. *Z. Kristallogr. - Cryst. Mater.* **1995**, *210*, 878.

(12) Douglass, R. M.; Staritzky, E. Crystallographic Data. 131. Uranium(IV)Pyrophosphate, UP_2O_7, Orthorhombic Form. *Anal. Chem.* **1956**, *28*, 1211−1212.

(13) Podor, R.; Francois, M.; Dacheux, N. Synthesis, Characterization, and Structure Determination of the Orthorhombic $U_2(PO_4)(P_3O_{10})$. *J. Solid State Chem.* **2003**, *172*, 66−72.

(14) Zachariasen, W. H. Crystal Chemistry of the 5f elements. *Actinide Elements* **1954**, 769−796.

(15) Alekseev, E. V.; Suleimanov, E. V.; Chuprunov, E. V.; Marychev, M. O.; Ivanov, V. A.; Fukin, G. K. Crystal structure and nonlinear optical properties of the $K_2UO_2(SO_4)_2\cdot{}_2H_2O$ compound at 293 K. *Crystallogr. Rep.* **2006**, *51*, 29−33.

(16) Read, C. M.; Morrison, G.; Yeon, J.; Smith, M. D.; zur Loye, H.-C. $A_2MnU_3O_{11}$ (A = K, Rb) and $Li_{3.2}Mn_{1.8}U_6O_{22}$: Three New Alkali-Metal Manganese Uranium(VI) Oxides Related to Natrotantite. *Inorg. Chem.* **2015**, *54*, 6993−6999.

(17) Wylie, E. M.; Burns, P. C. Crystal structures of six new uranyl selenate and selenite compounds and their relationship with uranyl mineral structures. *Can. Mineral.* **2012**, *50*, 147−157.

(18) Judd, B. R. Low-lying levels in certain actinide atoms. *Phys. Rev.* **1962**, *125*, 613.

(19) Kindra, D. R.; Evans, W. J. Magnetic Susceptibility of Uranium Complexes. *Chem. Rev.* **2014**, *114*, 8865−8882.

(20) Boudreaux, E. A.; Mulay, L. N. *Theory and Applications of Molecular Paramagnetism*; Wiley: New York, 1976.

(21) Mortl, K. P.; Sutter, J. P.; Golhen, S.; Ouahab, L.; Kahn, O. Structure and Magnetic Characteristics of an Oxalate-Bridged U(IV)-Mn(II) Three-Dimensional Network. *Inorg. Chem.* **2000**, *39*, 1626−1627.

(22) Yeon, J.; Smith, M. D.; Tapp, J.; Möller, A.; zur Loye, H.-C. Mild Hydrothermal Crystal Growth, Structure, and Magnetic Properties of Ternary U(IV) Containing Fluorides: $LiUF_5$, KU_2F_9, $K_7U_6F_{31}$, $RbUF_5$, RbU_2F_9, and RbU_3F_{13}. *Inorg. Chem.* **2014**, *53*, 6289−6298.

(23) Hubschle, C. B.; Sheldrick, G. M.; Dittrich, B. ShelXle: a Qt graphical user interface for SHELXL. *J. Appl. Crystallogr.* **2011**, *44*, 1281−1284.

(24) Sheldrick, G. M. A short history of SHELX. *Acta Crystallogr., Sect. A: Found. Crystallogr.* **2008**, *64*, 112−122.

(25) Dolomanov, O. V.; Bourhis, L. J.; Gildea, R. J.; Howard, J. A. K.; Puschmann, H. OLEX2: a complete structure solution, refinement and analysis program. *J. Appl. Crystallogr.* **2009**, *42*, 339−341.

(26) Bray, T. H.; Sullens, T. A.; Shvareva, T. Y.; Sykora, R. E.; Haire, R. G.; Albrecht-Schmitt, T. E. Product evolution in the Np(IV) fluorophosphate system. *J. Solid State Chem.* **2007**, *180*, 70−74.

(27) Morrison, G.; zur Loye, H.-C. Simple correction for the sample shape and radial offset effects on SQUID magnetometers. Magnetic measurements on Ln_2O_3 (Ln = Gd, Dy, Er) standards. *J. Solid State Chem.* **2015**, *221*, 334−337.

(28) Yeon, J.; Smith, M. D.; Sefat, A. S.; Tran, T. T.; Halasyamani, P. S.; zur Loye, H.-C. $U_3F_{12}(H_2O)$, a noncentrosymmetric uranium(IV) fluoride prepared via a convenient in situ route that creates U^{4+} under mild hydrothermal conditions. *Inorg. Chem.* **2013**, *52*, 8303−8305.

(29) Benard, P.; Louer, D.; Dacheux, N.; Brandel, V.; Genet, M. $U(UO_2)(PO_4)_2$, a New Mixed-Valence Uranium Orthophosphate: Ab Initio Structure Determination from Powder Diffraction Data and Optical and X-ray Photoelectron Spectra. *Chem. Mater.* **1994**, *6*, 1049−1058.

(30) Mishra, A. K.; Murli, C.; Singhal, A.; Sharma, S. M. Pressure induced phase transition in $U_2O(PO_4)_2$. *J. Solid State Chem.* **2008**, *181*, 1240−1248.

(31) Benard-Rocherulle, P.; Louer, M.; Louer, D.; Dacheux, N.; Brandel, V.; Genet, M. Structure Determination of Uranium Halogenide Phosphates $UXPO_4 \cdot {}_2H_2O$ (X = Cl, Br) from Powder Diffraction Data. *J. Solid State Chem.* **1997**, *132*, 315−322.

DOI: 10.1021/acs.inorgchem.8b01284
Inorg. Chem. XXXX, XXX, XXX−XXX